DIGITAL ACCESS TO SCHOLARSHIP AT HARVARD
DASH.HARVARD.EDU

HARVARD LIBRARY
Office for Scholarly Communication

Heteroepitaxy of \(La_2O_3\) and \(La_{2-x}Y_xO_3\) on GaAs (111)A by Atomic Layer Deposition: Achieving Low Interface Trap Density

Citation
Wang, Xinwei, Lin Dong, Jingyun Zhang, Yiqun Liu, Peide D. Ye, and Roy Gerald Gordon. Forthcoming. Heteroepitaxy of \(La_2O_3\) and \(La_{2-x}Y_xO_3\) on GaAs (111)A by atomic layer deposition: Achieving low interface trap density. Nano Letters.

Published Version
doi:10.1021/nl3041349

Permanent link
http://nrs.harvard.edu/urn-3:HUL.InstRepos:10265395

Terms of Use
This article was downloaded from Harvard University's DASH repository, and is made available under the terms and conditions applicable to Open Access Policy Articles, as set forth at http://nrs.harvard.edu/urn-3:HUL.InstRepos:dash.current.terms-of-use#OAP

Share Your Story

The Harvard community has made this article openly available.
Please share how this access benefits you. Submit a story .

Accessibility

Heteroepitaxy of La_2O_3 and $La_{2-x}Y_xO_3$ on GaAs (111)A by atomic layer deposition: achieving low interface trap density

Xinwei Wang[(1)(a)], *Lin Dong*[(2)], *Jingyun Zhang*[(2)], *Yiqun Liu*[(1)(b)], *Peide D. Ye*[(2)], *and Roy G. Gordon*[(1)]*

(1) Department of Chemistry and Chemical Biology, Harvard University, Cambridge, Massachusetts 02138, United States

(2) School of Electrical and Computer Engineering and Birck Nanotechnology Center, Purdue University, West Lafayette, Indiana 47906, United States

(a) Current address: School of Advanced Materials, Peking University Shenzhen Graduate School, Shenzhen 518055, China
(b) Current address: GLOBALFOUNDRIES, Inc., Malta, New York 12020, United States

Abstract: GaAs metal-oxide-semiconductor devices historically suffer from Fermi-level pinning, which is mainly due to the high trap density of states at the oxide/GaAs interface. In this work, we present a new way of passivating the interface trap states by growing an epitaxial layer of high-*k* dielectric oxide, $La_{2-x}Y_xO_3$, on GaAs(111)A. High-quality epitaxial $La_{2-x}Y_xO_3$ thin films are achieved by an *ex-situ* atomic layer deposition (ALD) process, and GaAs MOS capacitors made from this epitaxial structure show very good interface quality with small frequency dispersion and low interface trap densities (D_{it}). In particular, the La_2O_3/GaAs interface, which has a lattice mismatch of only 0.04%, shows very low D_{it} in the GaAs bandgap, below 3×10^{11} cm^{-2}eV^{-1} near the conduction band edge. The La_2O_3/GaAs capacitors also show the lowest frequency dispersion of any dielectric on GaAs. This is the first achievement of such low trap densities for oxides on GaAs.

Keywords: epitaxy, thin films, field-effect transistors, gallium arsenide

High-mobility InGaAs metal-oxide-semiconductor field-effect transistors (MOSFETs) have shown promising performance compared to Si-based devices for high-speed complementary MOS (CMOS) logic applications. However, GaAs MOS devices suffer from Fermi-level pinning, which is mainly due to the high trap density of states at the oxide/GaAs interface.[1, 2] In this work, we present a new way of passivating the interface trap states by growing an epitaxial layer of high-*k* dielectric oxide, $La_{2-x}Y_xO_3$, on GaAs(111)A, which effectively reduces the trap density and minimizes the frequency dispersion of capacitance.

For GaAs MOS structures, usually the dielectric oxide is either amorphous or polycrystalline, and therefore a high density of dangling bonds exists at the oxide/GaAs interface. These dangling bonds form interface states in the midgap,[3] which trap carriers and produce a large frequency dispersion of capacitance and Fermi-level pinning. GaAs MOS devices with epitaxial dielectric layers should have a low interface trap density of states (D_{it}), since a perfect epitaxial interface is supposed to have no dangling bonds. Also, contrary to polycrystalline oxides, a perfect epitaxial oxide should contain no grain boundaries,[4] which preserves the desired features of the low leakage current and uniformity. However, growing epitaxial oxides on GaAs is rather challenging, since GaAs is neither chemically stable nor thermally stable: GaAs can be oxidized easily to form low quality surface oxides that compromise the interface quality;[5] and GaAs starts to lose As over 400 ˚C.[6] Hong *et al.*[7, 8] have demonstrated a method of using *in-situ* electron beam evaporation to grow epitaxial $(Ga,Gd)_2O_3$ or Gd_2O_3 layers on GaAs(100) with the epitaxial relationships $(110)_{Gd2O3}//(100)_{GaAs}$, $[001]_{Gd2O3}//[011]_{GaAs}$, and $[-110]_{Gd2O3}//[01-1]_{GaAs}$. Their capacitance-voltage measurements do show a significant decrease in D_{it},[8] which suggests the importance of epitaxy in reducing interfacial defects.[9] However, the frequency dispersion of the capacitance was still fairly large,[8] and the drive current of the inversion-mode MOSFETs made from $(Ga,Gd)_2O_3$/GaAs was less than 1 mA/mm.[10] This may be due to the relatively

large in-plane mismatch between Gd_2O_3 and GaAs (1.9 % and -3.9% in the [011] and [01-1] directions of GaAs, respectively). Getting MOSFETs even of this quality also requires that there is no air-break between growth of the GaAs and the oxide, so that complex multi-chamber MBE systems are necessary. Several follow-up structural analyses of Gd_2O_3/GaAs(100)[11-13] revealed that perfect strained epitaxy only occurs in the first few layers. When the oxide film thickness exceeds ~3 nm, the Gd_2O_3 film starts to relax by generating misfit dislocations, so that the film is no longer perfectly epitaxial.[8] Unfortunately, simply substituing Gd_2O_3 with other lanthanide sesquioxides cannot accommodate the mismatch simultaneously in two orthogonal in-plane directions, since the in-plane lattice spacing of Gd_2O_3 is greater than GaAs in one direction but smaller in the other. Very recently, epitaxial growth of cubic high-*k* oxide, $LaLuO_3$, on GaAs(111)A has been achieved by an *ex-situ* atomic layer deposition (ALD) process in our group.[14] The heteroepitaxy relationship was found to be $(111)_{LaLuO3}//(111)_{GaAs}$ ($a_{LaLuO3} \approx 2a_{GaAs}$) with a relaxed interface.[14] Since the (111) plane has a three-fold symmetry, the in-plane mismatch between oxide and GaAs can be simultaneously engineered with lanthanide sesquioxides that have appropriate cation sizes. Initial electrical characterizations showed quite promising results, as the MOS capacitors made from epitaxial ALD $LaLuO_3$/GaAs showed an order of magnitude reduction in interface trap density (D_{it} ~7×10^{11} cm^{-2} eV^{-1}) compared with amorphous ALD Al_2O_3/GaAs (~8×10^{12} cm^{-2} eV^{-1}).[14] But, still $LaLuO_3$ has a fairly large lattice mismatch with respect to GaAs (-3.8%), and another concern is that Lu is one of the rarest elements on earth, which would be problematic for large scale fabrication.

In this work, we report an ALD process for depositing another high-*k* oxide, $La_{2-x}Y_xO_3$, epitaxially on GaAs(111)A. The *k* value of $La_{2-x}Y_xO_3$ was reported as high as 27,[15] and the terrestrial elemental abundance of Y is much higher than Lu. The ternary oxide, $La_{2-x}Y_xO_3$, can be considered as a mixture of La_2O_3 and Y_2O_3. The lattice constant of cubic La_2O_3 is very

slightly larger than 2 times the GaAs lattice constant, while the lattice constant of cubic Y_2O_3 is ~6% smaller than that of La_2O_3. Therefore, we can adjust the lattice constant of the ternary compound, $La_{2-x}Y_xO_3$, to study the effect of mismatch by varying the ratio of La and Y. As an ALD process grows films in a layer-by-layer manner, the compositional ratio of these two cations can be tuned by varying the ratio of La_2O_3 and Y_2O_3 cycles. A high-resolution X-ray structural analysis indicates a high-quality heteroepitaxy of $La_{2-x}Y_xO_3$ on GaAs(111)A. Electrical measurements on MOS capacitors show a promisingly small frequency dispersion of capacitance and a low D_{it} ~2×10^{11} $cm^{-2}eV^{-1}$ in the GaAs bandgap close to the conduction band edge. In addition, our process tolerates an air-break between growth of the GaAs and ALD of the epitaxial oxide. ALD is known to produce uniform films over large areas with good reproducibility,[16] so we believe that this process is very promising for large scale manufacturing.

$La_{2-x}Y_xO_3$ films were grown by ALD from precursors including lanthanum tris(*N*,*N*'-diisopropylformamidinate), yttrium tris(*N*,*N*'-diisopropylacetamidinate) and H_2O in a home-built tube reactor. In particular, pure La_2O_3 or pure Y_2O_3 films can be made by using the corresponding single metal precursor source. When films were deposited on amorphous SiN_x substrates, the as-deposited pure La_2O_3 and pure Y_2O_3 films were polycrystalline in their cubic phases, respectively. But alloying these two oxides did not form a polycrystalline film on amorphous SiN_x, on which the $La_{1.1}Y_{0.9}O_3$ film was almost amorphous (Supporting Information Figure S1). However, when $La_{2-x}Y_xO_3$ films were grown on GaAs (111)A, the as-deposited films, including La_2O_3, $La_{1.8}Y_{0.2}O_3$, $La_{1.1}Y_{0.9}O_3$ and Y_2O_3 were all well crystallized and, in fact, they were highly epitaxial due to induction by the substrates. Cross-sectional transmission electron microscopy (TEM) of $La_{2-x}Y_xO_3$/GaAs interfaces indicates a cube-on-cube epitaxy with a twin boundary relation at the interface, and the interface is atomically abrupt with no interlayer. A representative TEM image of a $La_{1.8}Y_{0.2}O_3$/GaAs(111)A sample

is shown in Figure 1a. The twin boundary relation at the oxide/GaAs was also confirmed by the selective area electron diffraction pattern as shown in Figure 1b, where the two sets of diffraction patterns belonging to cubic-phase $La_{1.8}Y_{0.2}O_3$ and GaAs are well aligned vertically. Especially, the diffraction spot of GaAs (111) overlaps with the $La_{1.8}Y_{0.2}O_3$ (222) spot, suggesting that the cubic lattice constant of $La_{1.8}Y_{0.2}O_3$ is very close to twice that of GaAs. However, TEM does not have enough resolution to determine precisely the small difference between their lattice constants. Therefore, high-resolution X-ray diffraction (HRXRD) was used to investigate the detailed epitaxial structures.

Coupled 2θ-ω HRXRD scans were performed for the oxide/GaAs(111)A samples. The peaks from the GaAs substrate were used as the internal references, and the oxide/GaAs lattice mismatch, which is defined as $(a_{\text{oxide}} - 2a_{\text{GaAs}})/2a_{\text{GaAs}}$, was calculated from the relative shift of the oxide peak with respect to the GaAs peak, assuming a fully relaxed heteroepitaxy relation at the interface.[14] For the $La_{1.1}Y_{0.9}O_3$/GaAs sample, the coupled 2θ-ω scan clearly shows both peaks of the GaAs(111) and $La_{1.1}Y_{0.9}O_3$(222) reflections, as shown in Figure 2a. The corresponding ω rocking curves of GaAs(111) and $La_{1.1}Y_{0.9}O_3$(222) reflections have a similar shape with the same full width at half maximum of ~32” (Supporting Information Figure S3). This indicates a high quality heteroepitaxy of $La_{1.1}Y_{0.9}O_3$/GaAs over a large area (several mm^2). The 2θ angle of the $La_{1.1}Y_{0.9}O_3$ (222) peak was found to be 0.958˚ greater than that of the GaAs(111) peak, which corresponds to a lattice mismatch of -3.32% for $La_{1.1}Y_{0.9}O_3$ with respect to GaAs. For the $La_{1.8}Y_{0.2}O_3$/GaAs sample, the 2θ-ω scan (Figure 2b) shows that the peaks of GaAs(111) and $La_{1.8}Y_{0.2}O_3$(222) are much closer, indicating $La_{1.8}Y_{0.2}O_3$ has a smaller lattice mismatch to GaAs. Thus, we performed a 2θ-Δω reciprocal space mapping (RSM) on this sample, and the RSM contour is plotted in the inset of Figure 2b, where the contour levels are chosen to highlight the peaks. The 2θ angle of the $La_{1.8}Y_{0.2}O_3$ (222) peak was found to shift by +0.18˚ from the GaAs(111) peak, indicating a lattice

mismatch of -0.64% for $La_{1.8}Y_{0.2}O_3$ with respect to GaAs. As for the La_2O_3/GaAs sample, the peaks of GaAs(111) and La_2O_3(222) in the 2θ-ω scan were found to be entirely overlapping with each other (Supporting Information Figure S4). Therefore, we performed another 2θ-ω scan around the GaAs(333) reflection to determine the mismatch with greater sensitivity. As shown in Figure 2c, the 2θ angle of the La_2O_3(666) peak was only ~0.046° smaller than that of the GaAs(333) peak, suggesting a much smaller lattice mismatch of only +0.04% for La_2O_3 with respect to GaAs.

In summary of the above structural analysis, both of the TEM and HRXRD results suggested a high-quality heteroepitaxy relation of $La_{2-x}Y_xO_3$/GaAs(111)A (x = 0, 0.2 and 0.9) with smaller lattice mismatch for higher La-content oxide. The measured lattice mismatch approximately follows Vegard's law (Supporting Information Figure S6). In addition, we also found that pure Y_2O_3 on GaAs(111)A is also epitaxial (Supporting Information Figure S5). Therefore we believe that epitaxy can be achieved for mixed $La_{2-x}Y_xO_3$ oxides with any La:Y ratio. This epitaxial relation is quite similar to the $LaLuO_3$/GaAs(111)A case, where the $LaLuO_3$ film was grown by a similar ALD process in our lab.[14]

Since epitaxial $La_{2-x}Y_xO_3$/GaAs structures are expected to provide a better interface quality with a lower interface trap density for electrical devices, we fabricated the corresponding $La_{2-x}Y_xO_3$/GaAs MOS capacitors to examine the electrical properties. Both p-type and n-type MOS capacitors of $La_{2-x}Y_xO_3$/GaAs(111)A (x = 0, 0.2 and 0.9) were fabricated and characterized by capacitance-voltage (C-V) and conductance-voltage (G-V) methods. Due to the hygroscopic nature of $La_{2-x}Y_xO_3$, an *in-situ* ALD capping layer of 6.5 nm Al_2O_3 was deposited right after the deposition of $La_{2-x}Y_xO_3$ on GaAs(111)A. Capacitors with only amorphous ALD Al_2O_3 as the dielectric material (Al_2O_3/GaAs(111)A) were also fabricated for comparison. The C-V response was measured at room temperature with the frequency of the small AC signal ranging from 1 kHz to 1 MHz. Figure 3 shows the

normalized C-V curves measured on these capacitors. A general trend for the frequency dispersion is that the capacitors with amorphous Al_2O_3 dielectric show the largest frequency dispersions compared with the capacitors with epitaxial $La_{2-x}Y_xO_3$ dielectric. Among these $La_{2-x}Y_xO_3$ capacitors, those with smaller lattice-mismatch $La_{2-x}Y_xO_3$ (higher La content) show smaller frequency dispersion. For p-type GaAs MOS capacitors, the frequency dispersion in the accumulation region ($\Delta C/C_{max}$) is reduced from 7.6% to ~2% by replacing the amorphous Al_2O_3 with epitaxial $La_{2-x}Y_xO_3$ as the dielectric (2.5%, 1.9% and 2.6% for x = 0.9, 0.2 and 0, respectively), and with a better lattice-matched oxide, La_2O_3, the dispersion in the depletion region (V_G~0) is further reduced. A similar trend was also observed for the n-type GaAs MOS capacitors: Al_2O_3 shows the largest frequency dispersion of 19.0% in the accumulation region, and $La_{1.1}Y_{0.9}O_3$, $La_{1.8}Y_{0.2}O_3$, and La_2O_3 show decreasing frequency dispersions of 18.6%, 15.6%, and 9.9%, respectively. We also measured the D_{it} by the conductance-voltage method (Supporting Information Figure S7).[17] The distribution of D_{it} within the GaAs band gap is plotted in Figure 4. Consistent with the C-V results, the interface of the amorphous Al_2O_3/GaAs showed much larger interface trap density compared to the epitaxial $La_{2-x}Y_xO_3$/GaAs interfaces. Among these epitaxial $La_{2-x}Y_xO_3$/GaAs devices, the La_2O_3/GaAs capacitor with a lattice-almost-matched interface showed the smallest D_{it} on the order of 10^{11} cm^{-2} eV^{-1}, and in particular, the interface trap density in the upper half of the band gap is below 3×10^{11} cm^{-2} eV^{-1} in the whole region measured. Notice that typically the D_{it} close to the conduction band edge is quite high for other oxides on GaAs, and those traps severely pin the Fermi level. The traps hinder the Fermi level from moving away from the center of the bandgap up to the conduction band edge, preventing the realization of high-performance inversion-mode GaAs MOSFETs. With a lattice-matched La_2O_3 dielectric layer, a very good interface with low trap density was achieved. The decreasing trend of D_{it} with smaller lattice mismatch indicates the importance of matching the lattice constant of the oxide with GaAs. In addition, the k values of $La_{1.1}Y_{0.9}O_3$, $La_{1.8}Y_{0.2}O_3$, and La_2O_3 were estimated from the

capacitance to be 20, 22, and 16, respectively. The above excellent electrical results show that the epitaxial $La_{2-x}Y_xO_3$ is a very promising gate dielectric candidate material for future high-performance GaAs MOS devices. In addition, we believe that the strategy of using epitaxial dielectrics can also be extended to other substrate material systemes, such as Ge, InP, and InGaAs.[18]

Conclusions. In this letter, we demonstrated an *ex-situ* ALD process for growing epitaxial $La_{2-x}Y_xO_3$ on GaAs(111)A. High-quality epitaxy of $La_{2-x}Y_xO_3$/GaAs(111)A was achieved for $x = 0$ (*i.e.* pure La_2O_3), 0.2 and 0.9. GaAs MOS capacitors made from this epitaxial structure showed very good interface quality with small frequency dispersion and low interface trap densities. In particular, the La_2O_3/GaAs interface, which has a lattice mismatch of only 0.04%, showed very low D_{it} in the GaAs bandgap, below 3×10^{11} $cm^{-2}eV^{-1}$ near the conduction band edge. The La_2O_3/GaAs capacitors also showed the lowest frequency dispersion of any dielectric on GaAs. This is the first achievement of such low trap densities for oxides on GaAs. We believe that these new results will expand the nearly 50-year research on the oxide/GaAs interface to an unprecedented level.

Methods. La_2O_3 and $La_{2-x}Y_xO_3$ films were grown by ALD from precursors including lanthanum tris(*N*,*N*'-diisopropylformamidinate), yttrium tris(*N*,*N*'-diisopropylacetamidinate) and H_2O in a home-built tube reactor. The pure La_2O_3 films were deposited by alternately supplying the La precursor vapor and water at a deposition temperature of 385 ˚C, and the ternary $La_{2-x}Y_xO_3$ oxides were deposited by repeatedly growing one or multiple cycles of La_2O_3 followed by one or multiple cycles of Y_2O_3 at 300 ˚C. Details of these ALD processes can be found in our previous publications.[19-20] The exposures of the La and Y precursors were estimated to be 0.003 Torr s and the exposure of H_2O was 0.06 Torr s in each cycle. After each H_2O pulse, the chamber was purged under nitrogen flowing for 80 s to minimize the

amount of water and/or hydroxyl groups trapped in the oxide films,[21] as they considerably degrade the crystallinity and permittivity and cause large frequency dispersion.[15] By controlling the cycle ratio of La_2O_3 and Y_2O_3, the elemental composition of the ternary oxide $La_{2-x}Y_xO_3$ (*i.e.* x) can be tuned. In this letter, two cycle ratios of $(La:Y)_{cyc} = 1:3$ and 3:1 were used, and their compositional ratios, which were determined by Rutherford backscattering spectroscopy, were $(La:Y)_{comp} = 1.1:0.9$ and 1.8:0.2, respectively. Before depositing $La_{2-x}Y_xO_3$ on the GaAs(111)A substrates, all the GaAs substrates were first dipped into a 3M HCl solution to remove the native oxide and then soaked in a 10% $(NH_4)_2S$ solution for 20 min for sulfur-passivation. Cross-sectional TEM images were taken with JEOL 2100. HRXRD spectra were taken by a Bruker D8 HRXRD with the incident beam Cu Kα1 being monochromated by a Ge (022) × 4 asymmetric monochromator. Due to the hygroscopic nature of $La_{2-x}Y_xO_3$, all the films for HRXRD analysis were capped by a 6 nm *in-situ* ALD Al_2O_3 layer before being taken out from the deposition chamber. For characterizing the electrical properties, n-type and p-type GaAs(111)A wafers with doping concentration of $5\text{-}7\times10^{17}cm^{-3}$ were used as the substrates. To fabricate MOS capacitors, either 7.5 nm $La_{2-x}Y_xO_3$ (for $x = 0.9$ and 0.2) or 9 nm La_2O_3 was first deposited on the GaAs substrates, and then an *in-situ* ALD layer of 6.5 nm Al_2O_3 was deposited on top to prevent the hygroscopic $La_{2-x}Y_xO_3$ from being exposed to air. All the $La_{2-x}Y_xO_3$/GaAs capacitors were subjected to rapid thermal annealing (RTA) at 800 ˚C for 30 s in N_2 ambient. Capacitors with amorphous ALD Al_2O_3 as the dielectric material (Ni/8nm Al_2O_3/GaAs(111)A) were fabricated for comparison. The Al_2O_3/GaAs(111)A capacitors were subjected to RTA at 600 ˚C for 30 s in N_2 ambient. Ni/Au circular electrodes for MOS capacitors were patterned by a lift-off process with a diameter of 150 μm. The capacitance-voltage/conductance-voltage measurements were carried out at room temperature by using an HP4284A precision LCR meter with frequency varying from 1kHz to 1MHz.

Associated Content

Supporting Information

TEM images and electron diffraction patterns for $La_{2-x}Y_xO_3$ deposited on amorphous SiN_x, schematic illustration of $La_{2-x}Y_xO_3$/GaAs lattice overlay, additional HRXRD scans including ω rocking scans for $La_{1.1}Y_{0.9}O_3$, coupled 2θ-ω scans for La_2O_3 and Y_2O_3, Vegard's law plot, frequency-dependent conductance-voltage plots and an extended D_{it} plot of $La_{1.8}Y_{0.2}O_3$/GaAs. This material is available free of charge via the Internet at http://pubs.acs.org

Author Information

Corresponding Author
*E-mail: gordon@chemistry.harvard.edu

Notes

The authors declare no competing financial interest.

Acknowledgements

The lanthanum and yttrium amidinate precursors were supplied by the Dow Chemical Company. This work was performed in part at Harvard University's Center for Nanoscale Systems (CNS), a member of the National Nanotechnology Infrastructure Network (NNIN). The work at Purdue University is partly supported by the Air Force Office for Scientific Research (AFOSR), monitored by Dr. James C.M. Hwang.

References

1. Oktyabrsky, S. and Ye, P. D. (Eds.), *Fundamentals of III-V Semiconductor MOSFETs*. Springer: 2010.
2. del Alamo, J. A. *Nature* **2011,** 479, (7373), 317-323.
3. Wang, W. C.; Xiong, K.; Wallace, R. M.; Cho, K. *J. Phys. Chem. C* **2010,** 114, (51), 22610-22618.
4. Shubhakar, K.; Pey, K. L.; Kushvaha, S. S.; O'Shea, S. J.; Raghavan, N.; Bosman, M.; Kouda, M.; Kakushima, K.; Iwai, H. *Appl. Phys. Lett.* **2011,** 98, (7).

5. Hinkle, C. L.; Milojevic, M.; Brennan, B.; Sonnet, A. M.; Aguirre-Tostado, F. S.; Hughes, G. J.; Vogel, E. M.; Wallace, R. M. *Appl. Phys. Lett.* **2009,** 94, (16).
6. Tsao, J. Y.; Brennan, T. M.; Klem, J. F.; Hammons, B. E. *J. Vac. Sci. Technol. A-Vac. Surf. Films* **1989,** 7, (3), 2138-2142.
7. Hong, M.; Passlack, M.; Mannaerts, J. P.; Kwo, J.; Chu, S. N. G.; Moriya, N.; Hou, S. Y.; Fratello, V. J. *J. Vac. Sci. Technol. B* **1996,** 14, (3), 2297-2300.
8. Hong, M.; Kwo, J.; Kortan, A. R.; Mannaerts, J. P.; Sergent, A. M. *Science* **1999,** 283, (5409), 1897-1900.
9. Hill, R. J. W.; Moran, D. A. J.; Xu, L.; Haiping, Z.; Macintyre, D.; Thoms, S.; Asenov, A.; Zurcher, P.; Rajagopalan, K.; Abrokwah, J.; Droopad, R.; Passlack, M.; Thayne, I. G. *Electron Device Letters, IEEE* **2007,** 28, (12), 1080-1082.
10. Ren, F.; Hong, M.; Hobson, W. S.; Kuo, J. M.; Lothian, J. R.; Mannaerts, J. P.; Kwo, J.; Chu, S. N. G.; Chen, Y. K.; Cho, A. Y. *Solid-State Electronics* **1997,** 41, (11), 1751-1753.
11. Sowwan, M.; Yacoby, Y.; Pitney, J.; MacHarrie, R.; Hong, M.; Cross, J.; Walko, D. A.; Clarke, R.; Pindak, R.; Stern, E. A. *Physical Review B* **2002,** 66, (20).
12. Kortan, A. R.; Hong, M.; Kwo, J.; Mannaerts, J. P.; Krajewski, J. J.; Kopylov, N.; Steiner, C.; Bolliger, B.; Erbudak, M. *J. Vac. Sci. Technol. B* **2001,** 19, (4), 1434-1438.
13. Hong, M.; Lu, Z. H.; Kwo, J.; Kortan, A. R.; Mannaerts, J. P.; Krajewski, J. J.; Hsieh, K. C.; Chou, L. J.; Cheng, K. Y. *Appl. Phys. Lett.* **2000,** 76, (3), 312-314.
14. Liu, Y.; Xu, M.; Heo, J.; Ye, P. D.; Gordon, R. G. *Appl. Phys. Lett.* **2010,** 97, (16).
15. Zhao, Y.; Kita, K.; Kyuno, K.; Toriumi, A. *Appl. Phys. Lett.* **2006,** 89, (25).
16. Kessels, W. M. M.; Putkonen, M. *MRS Bulletin* **2011,** 36, (11), 907-913.
17. Lin, D.; Brammertz, G.; Sioncke, S.; Fleischmann, C.; Delabie, A.; Martens, K.; Bender, H.; Conard, T.; Tseng, W. H.; Lin, J. C.; Wang, W. E.; Temst, K.; Vatomme, A.; Mitard, J.; Caymax, M.; Meuris, M.; Heyns, M.; Hoffmann, T. In *Enabling the high-performance InGaAs/Ge CMOS: a common gate stack solution*, Electron Devices Meeting (IEDM), 2009 IEEE International, 7-9 Dec. 2009; pp 1-4.
18. Urabe, Y.; Miyata, N.; Ishii, H.; Itatani, T.; Maeda, T.; Yasuda, T.; Yamada, H.; Fukuhara, N.; Hata, M.; Yokoyama, M.; Taoka, N.; Takenaka, M.; Takagi, S. In *Correlation between channel mobility improvements and negative V_{th} shifts in III-V MISFETs: Dipole fluctuation as new scattering mechanism*, Electron Devices Meeting (IEDM), 2010 IEEE International, 6-8 Dec. 2010; pp 6.5.1-6.5.4.
19. de Rouffignac, P.; Park, J.-S.; Gordon, R. G. *Chem. Mat.* **2005,** 17, (19), 4808-4814.
20. Wang, H.; Wang, J.-J.; Gordon, R.; Lehn, J.-S. M.; Li, H.; Hong, D.; Shenai, D. V. *Electrochem. Solid State Lett.* **2009,** 12, (4), G13-G15.
21. Kwon, J.; Dai, M.; Halls, M. D.; Langereis, E.; Chabal, Y. J.; Gordon, R. G. *J. Phys. Chem. C* **2009,** 113, (2), 654-660.

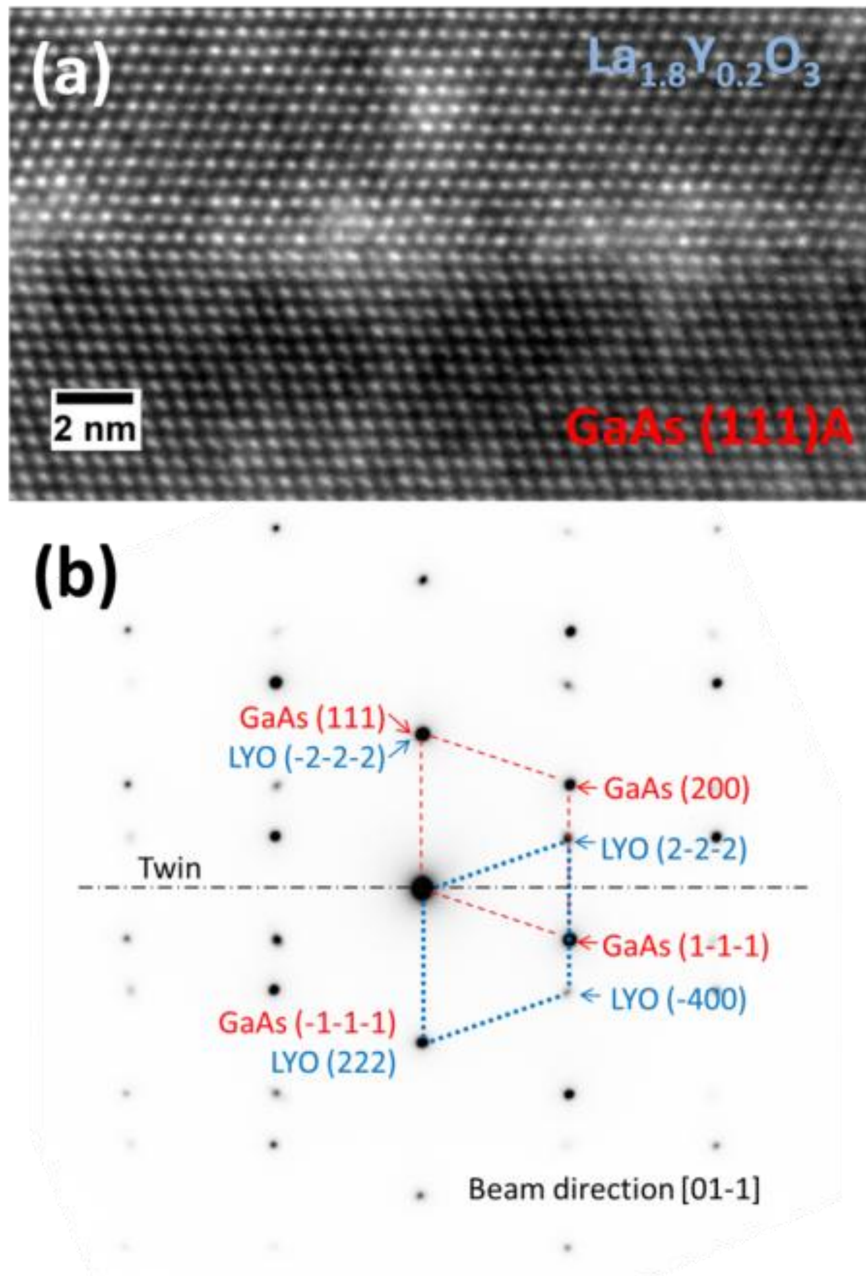

Figure 1. (a) Cross-sectional TEM image of $La_{1.8}Y_{0.2}O_3$/GaAs(111)A interface, and (b) the corresponding electron diffraction pattern with the electron beam aligned along the [01-1] direction of GaAs. ("$La_{1.8}Y_{0.2}O_3$" is labeled as "LYO" in the diffraction pattern.)

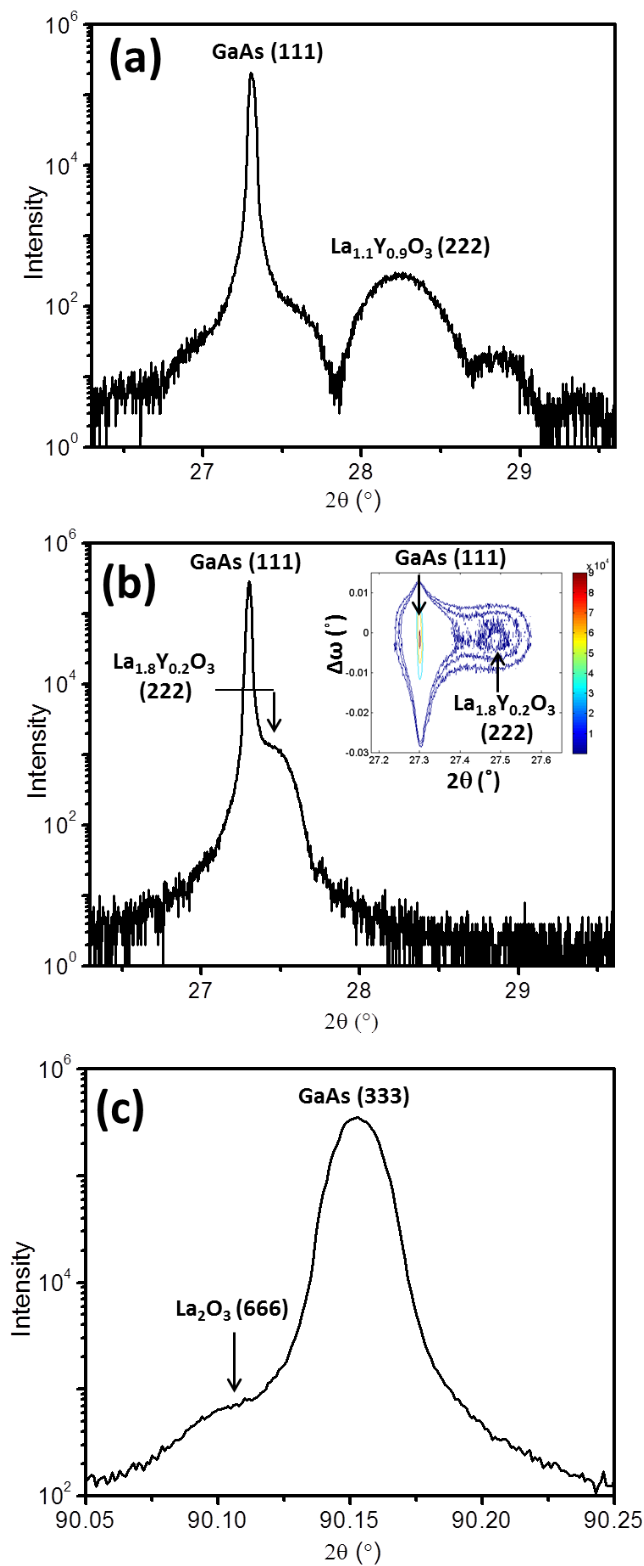

Figure 2. HRXRD coupled 2θ-ω scans of (a) $La_{1.1}Y_{0.9}O_3$, (b) $La_{1.8}Y_{0.2}O_3$ and (c) La_2O_3 on GaAs(111)A. The scans of (a) and (b) were performed around the GaAs (111) reflection, and the scan of (c) was performed around the GaAs (333) reflection. The inset of (b) shows the 2θ-Δω reciprocal space map around the GaAs(111) peak for the $La_{1.8}Y_{0.2}O_3$/GaAs sample.

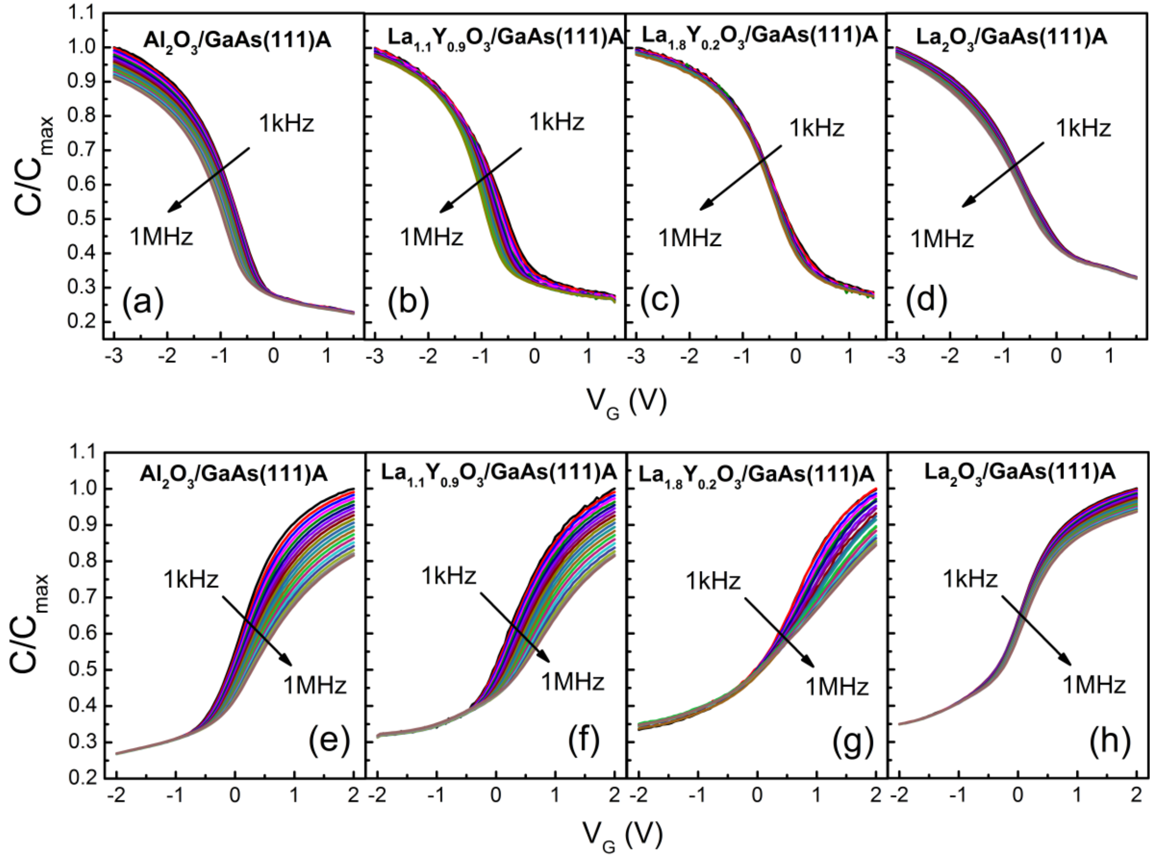

Figure 3. *C-V* characteristics of p-type and n-type GaAs MOS capacitors with stacks of (a, e) Ni/8nm Al_2O_3/GaAs(111)A, (b, f) Ni/6.5 nm Al_2O_3/7.5 nm $La_{1.1}Y_{0.9}O_3$/GaAs(111)A, (c, g) Ni/6.5 nm Al_2O_3/7.5 nm $La_{1.8}Y_{0.2}O_3$/GaAs(111)A, and (d, h) Ni/6.5 nm Al_2O_3/9 nm La_2O_3/GaAs(111)A, respectively.

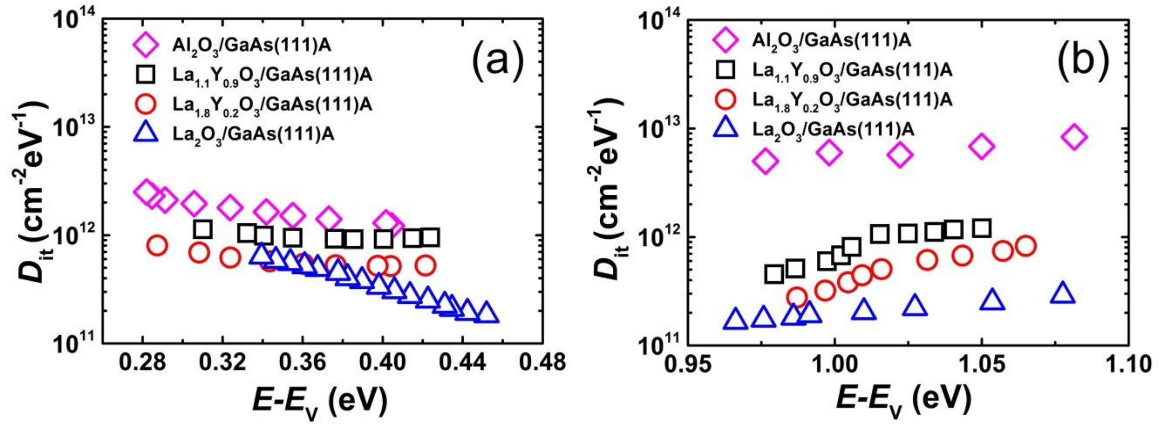

Figure 4. D_{it} distribution in the GaAs band gap obtained on both (a) p-type and (b) n-type MOS capacitors with Al_2O_3/GaAs(111)A, $La_{1.1}Y_{0.9}O_3$/GaAs(111)A, $La_{1.8}Y_{0.2}O_3$/GaAs(111)A and La_2O_3/GaAs(111)A as the interfaces, respectively.

TOC Graphic